PAPER

Four-port dual-band textile MIMO antenna for biomedical health monitoring systems: on-body mutual coupling reduction characterization

To cite this article: Hamza A Mashagba *et al* 2024 *Phys. Scr.* **99** 095026

Physica Scripta

PAPER

Four-port dual-band textile MIMO antenna for biomedical health monitoring systems: on-body mutual coupling reduction characterization

RECEIVED
21 December 2023

REVISED
29 July 2024

ACCEPTED FOR PUBLICATION
15 August 2024

PUBLISHED
29 August 2024

Hamza A Mashagba[1,2], **Hasliza A Rahim**[1,2,*], **Mohd Najib Mohd Yasin**[1,2], **Mohd Haizal Jamaluddin**[3], **Mohammad Tariqul Islam**[4], **Wazie M Abdulkawi**[5], **Arif Mawardi Ismail**[1,2], **Md. Moniruzzaman**[6] and **Samir Salem Al-Bawri**[7,*]

[1] Faculty of Electronic Engineering & Technology, Universiti Malaysia Perlis (UniMAP), 02600, Arau, Perlis, Malaysia
[2] Centre of Excellence for Advanced Communication Engineering (ACE), Universiti Malaysia Perlis (UniMAP), 01000, Kangar, Perlis, Malaysia
[3] Wireless Communication Centre, Faculty of Electrical Engineering, Universiti Teknologi Malaysia, Johor Bahru, 81310, Malaysia
[4] Department of Electrical, Electronic and Systems Engineering, Faculty of Engineering and Built Environment, Universiti Kebangsaan Malaysia, Bangi, 43600, Malaysia
[5] Electrical Engineering Dept., College of Engineering, Prince Sattam Bin Abdulaziz University, Wadi Addwasir, 11991, Saudi Arabia
[6] Dept. of Electrical and Electronics Engineering, College of Engineering and Technology, International University of Business Agriculture and Technology, Uttara, Dhaka, 1230, Bangladesh
[7] Space Science Center, Institute of Climate Change, Universiti Kebangsaan Malaysia (UKM), Bangi, 43600, Selangor, Malaysia
[*] Authors to whom any correspondence should be addressed.

E-mail: haslizarahim@unimap.edu.my **and** s.albawri@gmail.com

Keywords: antenna and propagation, array antennas, bioelectromagnetics, MIMO antenna, mutual coupling reduction, wearable antenna

Abstract

The paper outlines a methodology to diminish mutual coupling in 4-port dual-band MIMO textile antenna for biomedical applications. This antenna leverages MIMO technology and Wireless Body Area Network (WBAN) for operation in two distinct frequency bands at (3.5 & 2.45 GHz). The antenna is made up of four octagonal patch antennas, each having a bar and a split-ring (SR) slot with 47.2×31 mm^2 dimensions for each patch. A hybrid mutual coupling (MC) approach was investigated with closely spaced patches (up to 0.05λ). Various bending setups have been selected along with flat case to examine the antennas' resilience which demonstrate such agreement between measured and simulated findings. Furthermore, the MC is only −20 dB, the envelope correlation coefficient (ECC) is 0.001, and maximum peak measured gain of 5.2 dBi is achieved with lowest peak specific absorption rate (SAR) value. Even when bent at a 60° angle along with *y*-axis and *x*-axis, the antenna retains a decent gain of 1.861 dBi in the low frequency region and 5.479 dBi at high frequency band. Surprisingly, the antenna outperforms the attenuation produced by the lossy effects of the human body, indicating a favorable alignment between the modelled and observed findings.

1. Introduction

Nowadays, the trend in antenna development is moving towards more flexible formats, which is particularly attractive in wearable purposes, as wellness monitoring and tracking [1]. The requirement for these antennas to be wideband is further amplified by the need for users to move freely while wearing them without affecting their morphology. In addition, creating wearable antennas that allow for real-time data transfer with little loss is vital for monitoring critical diseases and operations. In the open literature, a lot of MIMO antennas for single port [2–5] and two ports MIMO [6–9] structures have been proposed ranging from 2 GHz to 38 GHz. However, the lack of MIMO antennas addresses another challenge for 5G since MIMO technology requires multiple array elements and multiple ports for its realization. The challenge stems from the need to accommodate a larger number of antenna components, leading to increased coupling effects, as a result, loss of antenna efficiency features [10]. The significance of four-port textile MIMO antennas in enhancing the capacity, coverage, and data

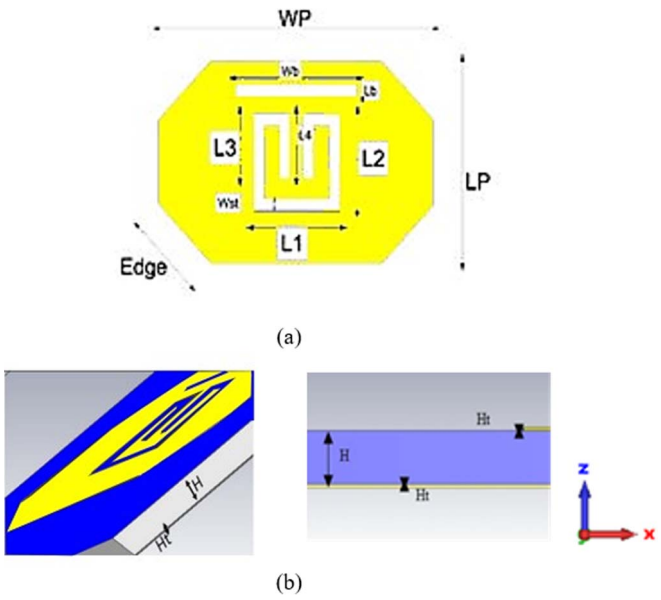

Figure 1. (a) Single element square slotted textile antenna Antenna dimensions with the gap added between L2 and L3, (b) 3D sigth the height of each layer

Table 1. Dimensions of the single patch for single-element dual-band antenna. Value (mm).

Parameter	Value	Parameter	Value	Parameter	Value	Parameter	Value
Lp	31	Ht	0.17	WL	0.73	Edge	9
Wp	47.2	WB	21	LL	60	LB	17
Ls	70	L1	15	LB	20		
Ws	70	L2	15	L1	15		
H	3	L3	10	L2	15		

rates of 5G networks, particularly in dense urban environments where on-body communication is critical [11]. Moreover, the unique characteristics of textile-based antennas make them well-suited for on-body applications, offering flexibility, comfort, and conformal integration with clothing. However, the lack of four-port textile MIMO antennas tailored specifically for textile substrates poses a challenge in realizing the full potential of on-body communication systems.

The degree of mutual interaction between the array antennas was controlled by the surface current distribution. To achieve compactness in MIMO antenna design while keeping high overall performance, the array parts of the antenna must be arranged as closely as feasible in practical design. The fundamental problem, nevertheless, is that the tightly spaced array of elements would result in higher radiation interactions [12]. Many researchers have lately researched MIMO antennas to draw attention to this challenge and have offered several solutions, such as faulty ground structures, metamaterial, and feeding network structures.

Up to the millimeter-wave spectrum, numerous low-frequency four-port MIMO antennas have been suggested [12, 13], Some designs, however, exclude the lower frequency bands for 5G. In [14], a basic planar tightly linked microstrip patch in a four-port MIMO configuration is shown, fed by a constructed right-lefthand integrated FM antenna; the suggested antenna had a bandwidth of (2.54 GHz) (1.36–3.9 GHz). Although wider bandwidths were achieved in these designs, the antennas were targeted solely for circularly polarized characteristics and provided higher MC (> -20 dB). Similarly, in [15], four symmetric monopole-radiating elements and four-port MIMO antenna with super wideband were proposed. The reported MC is quite high (> -25 dB). Numerous methods for reducing mutual coupling have been proposed in the literature. works. These approaches encompass alterations to the antenna configuration, such as integrating electromagnetic bandgap (EBG) structures [16, 17], incorporating slots [17], employing neutralization lines [18, 19] utilizing metamaterial arrangements [20] employing parasitic elements [12, 21] employing hybrid methodologies that merge defected ground plane structures (DGS) and stubs [22, 23], adopting split ring resonators (SRR) [24, 25], employing diagonal positioning of array elements [26, 27], and modifying the patch structure through truncation[28]. A comprehensive study on mutual coupling suppression techniques has been reported in [29, 30]

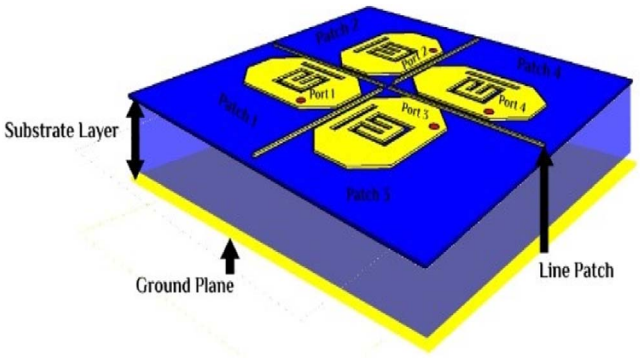

Figure 2. Perspective view with all port's locations.

Table 2. Dimensions of the four-port dual-band MIMO antenna.

h	Value	Parameter	Value	Parameter	Value	Parameter	Value
Lp	31	Ht	0.17	WL	0.73	Edge	9
Wp	47.2	WB	21	LL	60	LB	17
Ls	127.6	L1	15	LB	20		
Ws	132.8	L2	15	L1	15		
H	3	L3	10	L2	15		

Table 3. S11 and S21 summary for different antenna variations.

Rotation	Design	Freq (GHz)	S_{11} (dB)	S_{21} (dB)	S_{34} (dB)
	Stage 1	2.45	−12.37	−26.35	−27.8
		3.5	−25.88	−27.5	−22.8
					
	Stage 2	2.45	−16.35	−27.8	−29.71
		3.5	−39.1	−22.8	−22.81
					
	Stage 3	2.45	−13.5	−33.1	−35.3
		3.5	−26.6	−35.7	−40.7
					
	Stage 4	2.45	−14.2	−33.8	−33.8
		3.5	−30.5	−34.7	−36.7
					

In [31], To improve the isolation properties of a four-port MIMO antenna, meander line structures are inserted between the antenna parts. The antenna has a wideband frequency range of 2.74–4.41 GHz with an MC greater than −30 dB for all ports. In [13], integration of multiple antennas was realized with 2 × 2 MIMO configuration with operating frequency of 3.3–5 GHz. The antenna offered a wide bandwidth of 1.7 GHz, but the gain is low, 4.7 dB, with an unknown MC value. However, to the best of authors' knowledge, none has reported four-port MIMO textile antenna with dual-band frequency (2.45 and 3.5 GHz) that provides wide bandwidth and low MC (< −20 dB). In this article, a unique MIMO antenna structure has been offered providing a novel approach to mitigating mutual interference between two MIMO antennas. The primary goal is

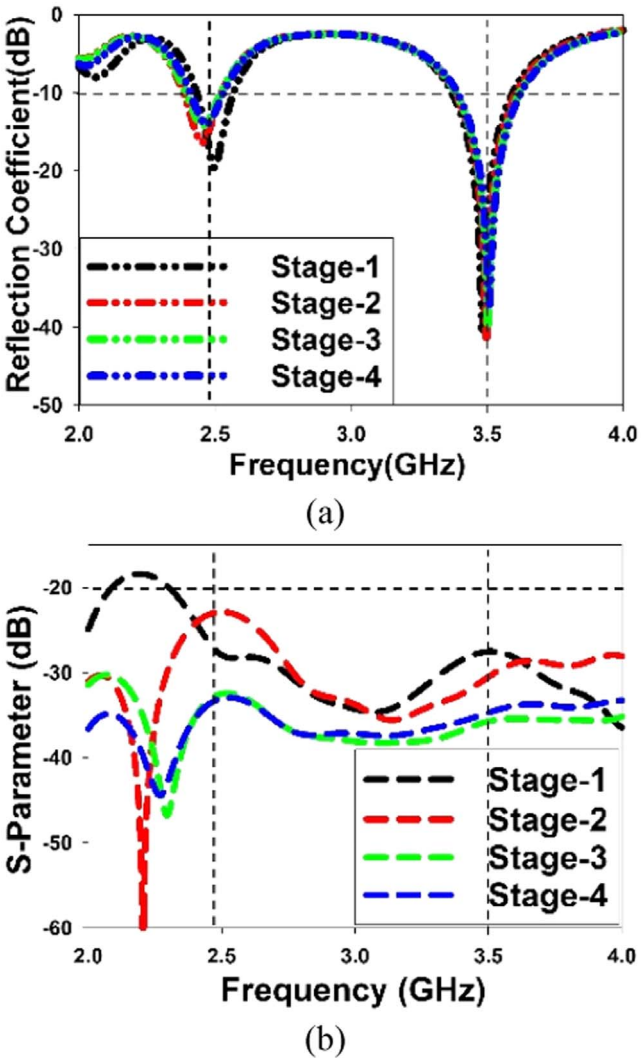

Figure 3. Simulation for the suggested MIMO with the hybrid technique and without. (a) S11 and (b) S21.

to achieve an S21 of less than −20 dB by positioning the antenna elements as close together as feasible, with a 0.05λ edge-to-edge spacing. A thorough study is performed to estimate the bending deformation resistance of the suggested MIMO antenna

The following is the structure of this paper: The proposed MIMO antenna's design and operation mechanism is followed by a three-part investigation of the MC effects on the antenna: The analysis includes evaluating the distance analysis, reducing mutual coupling, determining the realized gain, and assessing the cover correlation measurement. The findings of the model were documented and reported. in section 4, and the work finishes with section 5, which contains the conclusions.

2. Antenna configuration

2.1. Antenna element design

The proposed antenna is dual band in operation with a lower band at 2.45 GHz for WBAN and higher band at 3.5 GHz for 5G applications. Felt textile is chosen as the substrate for the antenna design due to its advantageous electrical, mechanical, and morphological properties, which are critical for ensuring high performance in wearable applications. Felt typically exhibits a low dielectric constant and loss tangent, which reduces dielectric losses and enhances antenna efficiency and bandwidth. This property is essential in wearable technology where minimizing energy loss is crucial for maintaining performance.

The Felt fabric as a substrate, is inserted by between an upper radiator and a full ground plane. The dielectric properties of Felt textile have a relative permittivity (r) of 1.44 and a loss tangent (tan) of 0.044 [32]. The direct experimental evidence of dielectric properties of Felt has been carried out in [33]. ShieldIt Super electro-textile from LessEMF Inc. is used for the conductive components, and it has an anticipated conduction, σ of 1.18×10^5

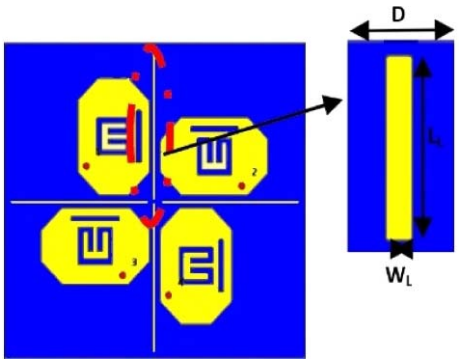

Figure 4. The MIMO antenna includes A-line patch.

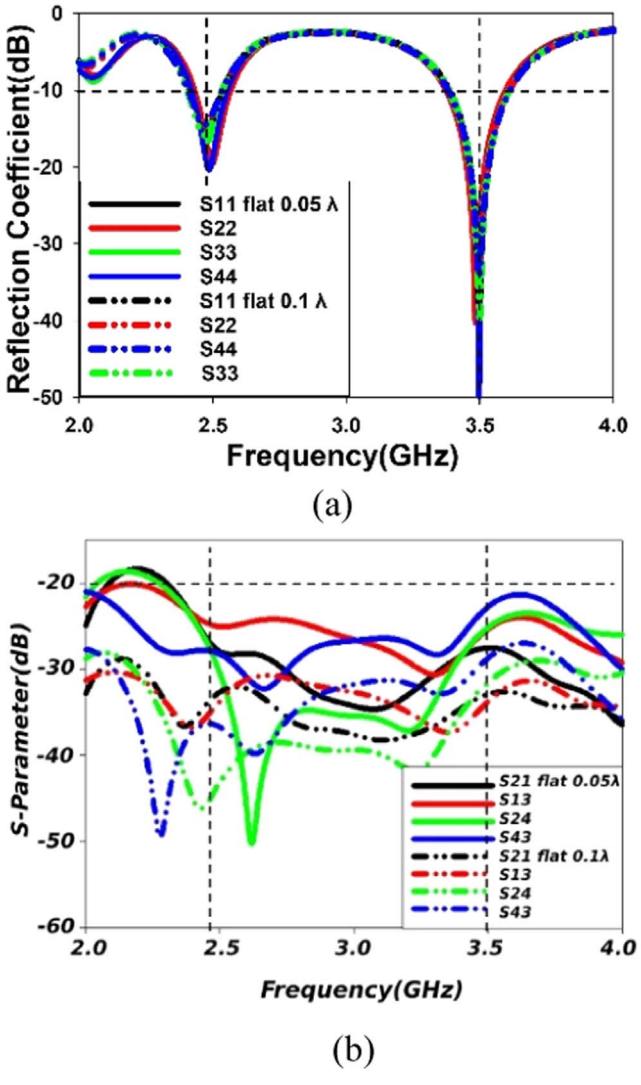

Figure 5. Antenna simulation results for various patch distances in λ (a) Sii and (b) Sij.

Sm-1. As indicated in figure 1, the total dimensions of the antenna are 132.8 × 127.6 mm^2, while the top radiator is 47.2 × 31 mm^2. CST Microwave Studio software is used for all simulations and improvements. The design parameter of single-element split-ring (SR) slotted textile antenna is tabulated in table 1.

In this design, the patch radiator is particularly designed to create resonance at 2.45 GHz, which serves as the lower band frequency. Then, the antenna was designed to generate an alternative echoing frequency at 3.5 GHz.

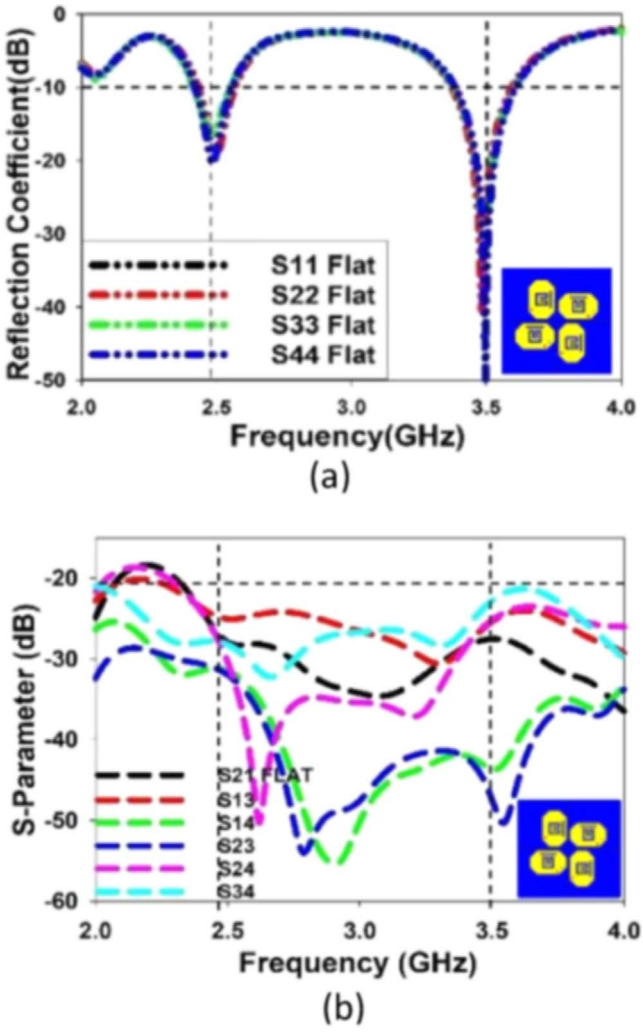

Figure 6. The results of the simulation for the patch antenna using the hybrid approach with a 0.05 λ gap (a) Reflection coefficient Sii and (b) MC Sij.

The presence of a SR slot in the rectangular patch antenna's center allows for enhanced bandwidth in the upper 3.5 GHz band.

The lower band, on the other hand, may be adjusted by varying the length of the SR (L1, L2 and L3), which works as a separate resonating slot for the lower frequency. The design process encompassed four distinct procedures, described in the following:

- The patch's dimensions were first determined without the SR -shaped slot and were based on the upper band resonance. After that, the probe feeding arrangement was fine-tuned for proper resistance matching in the top band.
- Following that, SR and bar slots were introduced to increase bandwidth and enable operation in the appropriate bands. Finally, the size of the SR slots was carefully adjusted to exhibit circular coupling behavior in the bottom band.

2.2. A four-port MIMO antenna

The proposal occurred to expand to include a 4-element flexible MIMO design configuration, namely a 2 × 2 MIMO antenna with 4 ports which is more difficult than designing a single or two-port MIMO antenna, owing to MC between antenna parts [15]. As illustrated in figure 2, the array consists of four-SR slot antennas with bar slots spaced at a space D2 from antenna edge A to B. The main antenna is designed in a way that controls MC between antenna elements using a hybrid method. A mixture approach, including a line patch and antenna element variation is used present in figure 2. The patches need to match, and the unadjusted patches need to be segregated in order to implement this solution. It is clear that there is no issue with the MC between neighboring

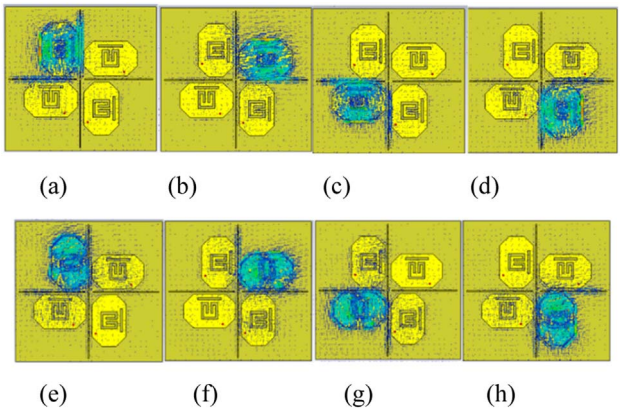

Figure 7. Surface current distribution for various configurations from ports 1–4 at 2.45 GHz (a), (b), (c), and (d) and 3.5 GHz (e), (f), (g), and (h).

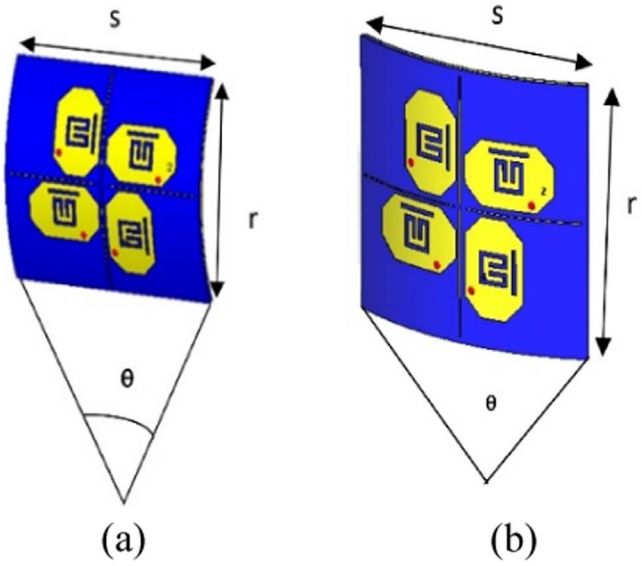

Figure 8. Patch antenna for bending curvature.

elements when using this technique. As a result, without experiencing any resonant frequency mismatches among S11, S22, S33, and S44, this technique efficiently mitigates MC.

Table 2 shows the important characteristics of the split-ring (SR) slotted MIMO antenna. The suggested textile MIMO antenna has overall dimensions of 132.8 × 127.6 mm^2 (132.8 × 127.6), with calculations based on a lower operating frequency of 2.45 GHz.

3. Antenna working principle

In order to comprehend the antenna's activity and how it functions as a result, several subsections will be discussed below, including the analysis of the current distribution movement along the conducted.

3.1. Design process

Upon the completion of the SR bar slotted two-port MIMO antenna design, the design is extended to a four-element structure to form a 1 × 2 MIMO antenna to a 2 × 2 MIMO antenna with four ports. Compared with single and two-port MIMO antennas, a four-port MIMO antenna design is more critical due to the MC of antenna elements [15]. The basic antenna is designed in such a way that it controls MC between antenna elements using the hybrid technique of MC. A hybrid technique involving a line patch and rotation of antenna elements is applied in this proposed MIMO antenna to achieve MC < -20 dB, as shown in figure 3 (a),(b). To

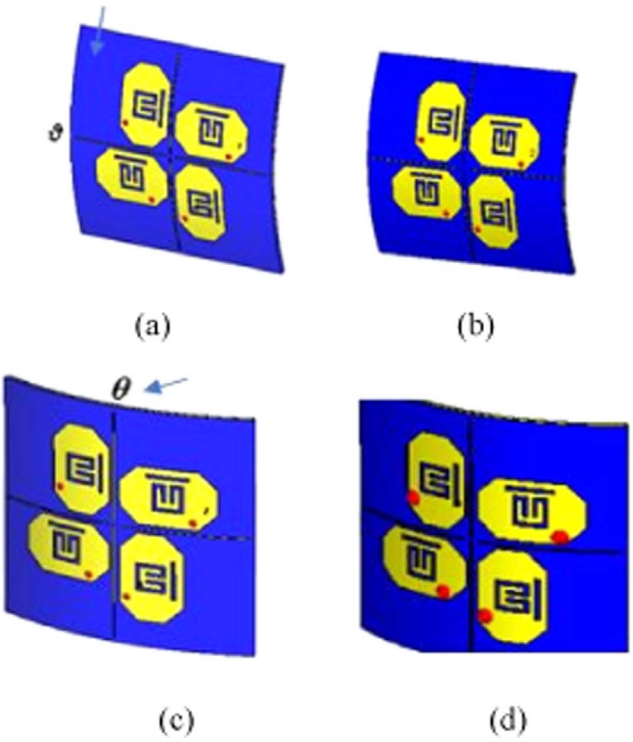

Figure 9. The suggested bending angles for MIMO are as follows: (a) bent at 45 degrees *x*-axis, (b) bent at 60 degrees *x*-axis, (c) bent at 45 degrees *y*-axis, and (d) bent at 60 degrees *y*-axis.

implement this solution, the patches must be matched, and unadjusted patches must be isolated. When using this solution, there is no problem with the MC between adjacent elements. Thus, this solution will suppress MC without any resonant frequency mismatch between S11, S22, S33, and S44 [34].

A detailed design procedure is present which can be summarized in four steps, as follows:

- First, the dimensions of the patch without an SR-shaped slot are calculated based on the upper band resonance.
- Second, the probe feed structure is optimized to obtain a suitable matching in the upper band.
- Third, the SR shape and the bar slot are added to broaden the bandwidth and provide operation in the respective bands.
- Fourth, the dimensions of the SR-shaped slot are tuned to provide operation in the respective lower band
- The overall dimension is of $132.8 \times 127.6\ mm^2$, whereas the top radiator is dimensioned at $47.2 \times 31\ mm^2$,

The placement of four elements antenna array orthogonally (vertical and horizontal direction) to reduce the MC is carried out and illustrated as the following:

- Place the bottom orthogonal two adjacent element arrays, as in table 3, with the line patch in vertical (between adjacent elements) and horizontal (between parallel elements at top and bottom) directions to separate each element array, as shown in table 3 (Stage 3), and without the line patch (Stage 4).
- Place the bottom two adjacent element arrays in an orthogonal structure, the third antenna element in a horizontal direction (Port 3), and the fourth antenna element is rotated 90° (Port 4) with line patches, as shown in table 3 (Stage 1), and without the line patch (Stage 2).

3.2. Distance analysis

The results show that the Sii and bandwidth for all ports are consistent in both lower and upper bands, according to figure 3. Still, as figure 3(b) illustrates, when the distance between the patches reduces, the Sij values increase, indicating tighter coupling between the patches. The gap between patch components has a significant impact on antenna efficiency, particularly regarding reflection coefficient and MC. Figure 4 depicts the effect of varying the

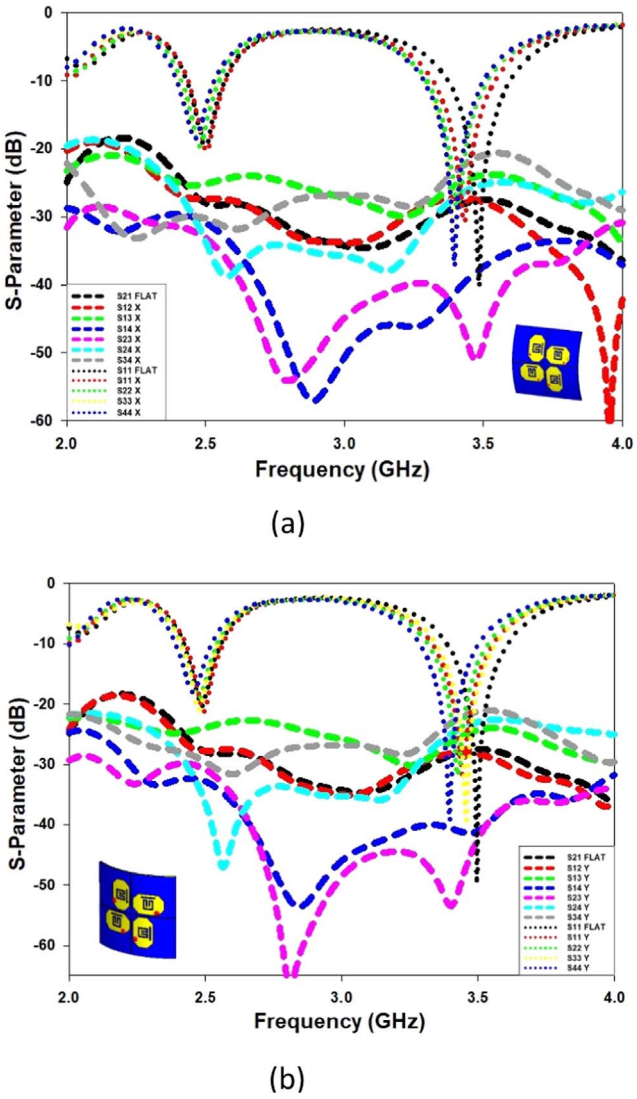

Figure 10. The intended MIMO antenna's function where the bending at $\theta = 60^{\circ}$ occurs at the x & y axes, respectively.

distance between the antennas of 0.05λ and 0.1λ. At (2.45 & 3.5 GHz), the MC rates increase from < -30 dB (0.1λ) to < -20 dB (0.05λ) as shown in figure 5. Thus, the closely spaced elements of 0.05λ are chosen and offered low MC of less than -20 dB for all MIMO configurations as shown in figure 6. Based on the analysis mentioned earlier, a four-port flexible MIMO textile structure has been designed.

It consists of an SR and bar-slotted MC reduction enhancement structure, with four-line patches positioned in opposite orthogonal arrangements for the upper and lower elements.

3.3. Surface current distribution (SCD)

In figure 7, the SCD is depicted when a single port is active. The illustration highlights the antenna components and demonstrates how introducing a line-patch between them or rotational the patch element can effectively minimize the undesired dealings with the nearby patch. But, in all scenarios, nevertheless, some electric current yet overflows to the adjoining patch. Using together strategies reduces MC between patch parts even more, as seen by a considerable drop in current overflow to the next patch. Techniques reduced the coupling between antenna parts significantly. To investigate the two resonant modes excited for the (2.45 & 3.5 GHz) bands, On the other hand, figure 7 illustrates the surface current distribution when one of the ports is excited. As seen in this figure, a hybrid technique of adding the line patch in between the antenna elements and rotating the patch element reduced the current interaction with the other patch element. However, a very low current might be overflowed to the adjacent patch. The combination of both techniques significantly reduced the coupling between the antenna elements.

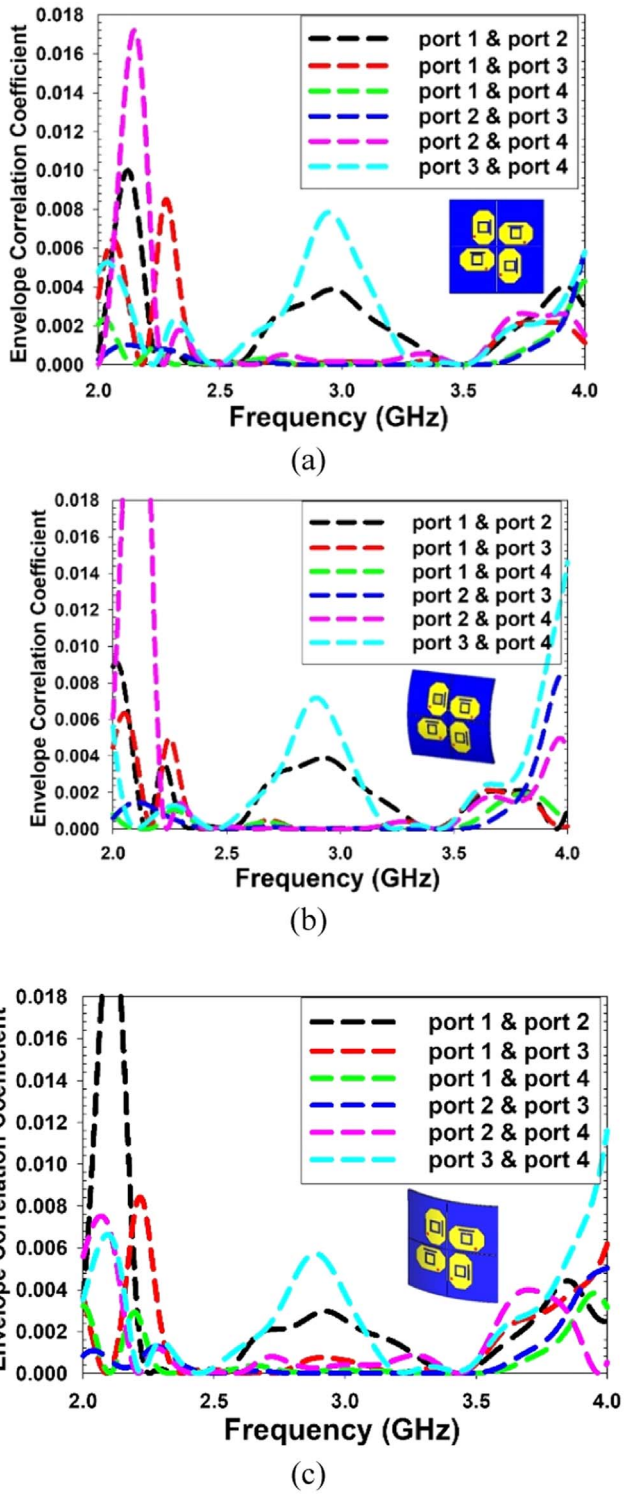

Figure 11. The ECC of the MIMO antenna when the bending $\theta = 60°$ (a) at the x-axis and (b) at the y-axis.

4. Results and discussions

4.1. Bending analysis

This section looks into how bending affects the suggested MIMO antenna. Achieving various bending angles for MIMO textile antennas on the human body involves innovative design and fabrication techniques tailored to the flexibility and conformability requirements of wearable applications. Researchers have employed advanced materials such as elastomers and conductive textiles with stretchable properties to enable the antenna to bend and conform to the contours of the body without compromising performance. Additionally, techniques like

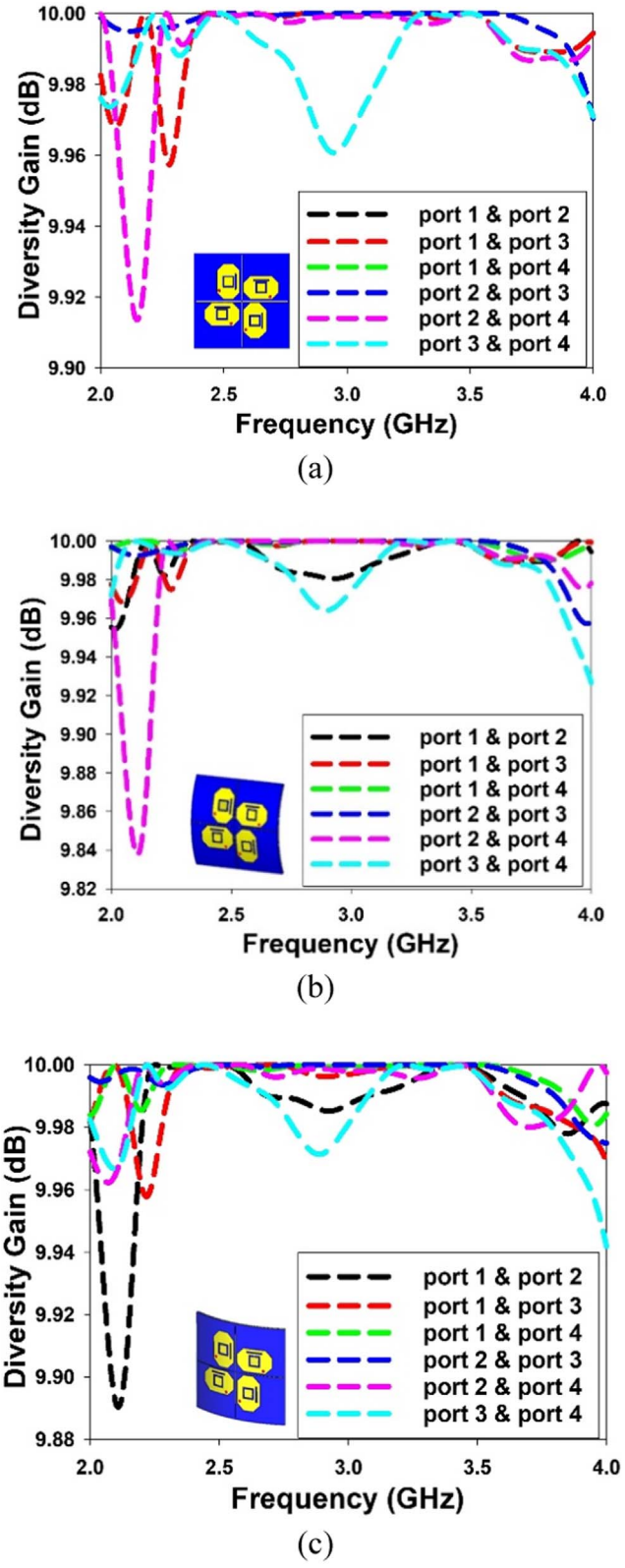

Figure 12. DG for the proposed MIMO antenna (a) Flat (b) bending $\theta = 60^{\circ}$ x-axis and (c) bending $\theta = 60^{\circ}$ y-axis.

origami-inspired folding patterns and 3D printing of flexible substrates have been utilized to create antennas capable of adapting to different bending angles while maintaining structural integrity and electrical performance. These approaches enable the practical implementation of MIMO textile antennas on the human body, providing reliable communication in diverse wearable scenarios.

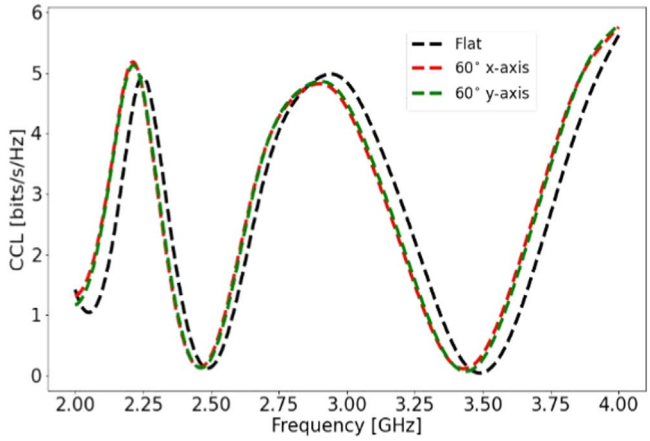

Figure 13. MIMO antenna CCL for flat and bending = 60°, *x*-axis and *y*-axis.

The antenna is expected to be fitted into a suit in a realistic on-body application, where it will be susceptible to bending. To evaluate the effects of bending, simulations are conducted at different angles (θ) ranging from 0° to 60°, corresponding to radii of 0, 507.2, 253.6, 169.1, and 126.8 mm, respectively, based on the given expression as seen in figure 8.

$$S = r\theta \tag{1}$$

where θ is the central angle measured in radians, r is the circle's radius, and S is the arc length. The parameters of θ are intended to approximate the bend of the suggested MIMO antenna as bound on the arm of a normal human body. Figure 9 shows the bending under two situations which curved at the y- axis and x-axis for five distinct curving angles. When the antenna is bent at the *y*-axis with a radius of = 60° @ 126. 8 mm, the most severe scenario occurs. Following that, measurements are carried out to monitor the function of the anticipated MIMO antenna in these circumstances. Figure 9 illustrates a comparison between the simulation results for the flat condition and the measurements obtained from the bent antennas.

Reducing the curving degree from 60° to 10° led to decrease in resonance for both frequency bands, although the change was further substantial in the higher band. However, bending the antenna at different degrees alongside the (x & y-axes) produced different (MC) behaviors. Lower S_{21} was reported to have increasing bending degrees when the antenna was bent by the *x*-axis at 2.45 GHz. At 3.5 GHz, however, the behavior was the inverse. Modifying the degree of bending along the *y*-axis yielded the opposite, resulting in fluctuating S21 values in the low-frequency band but relatively stable values in the higher-frequency band. When the antenna was bent at a 60° -degree angle, significant (MC) was observed in both frequency bands as shown in figure 10. Consequently, it concludes that altering the curving of the antenna at several scales significantly affects its functioning, particularly at 3.5 GHz.

4.2. Radiation efficiency gain and correlation analysis

The performance of the proposed MIMO antenna is evaluated using the Envelope Correlation Coefficient (ECC), Diversity Gain (DG), Channel Loss Capacity (CCL), and Total Active Reflection Coefficient (TARC). The ECC (e) and DG are calculated as follows using (2), which specifies the connection between analysis and antenna components in terms of channel correlation values:

$$\rho_e = \frac{|\vec{E}_i(\theta,\ \phi)\vec{E}_j(\theta,\ \phi)d\Omega|^2}{\iint|\vec{E}_i(\theta,\ \phi)|^2 \iint|\vec{E}_j(\theta,\ \phi)|^2 d\Omega} \tag{2}$$

When the ECC value is low, it suggests that the antenna elements have little correlation. The spatial correlation measurement amongst patch elements has a comparable effect on the DG. A little ECC value (0.5) leads to a significant diversity benefit, as follows:

$$DG = 10\sqrt{1 - \rho_e^2} \tag{3}$$

The simulated ECC throughout the significant frequency range is shown in figure 11. The ECC values are less than 0.001 at all resonant frequencies for both flat and bending situations, meeting the minimal diversity

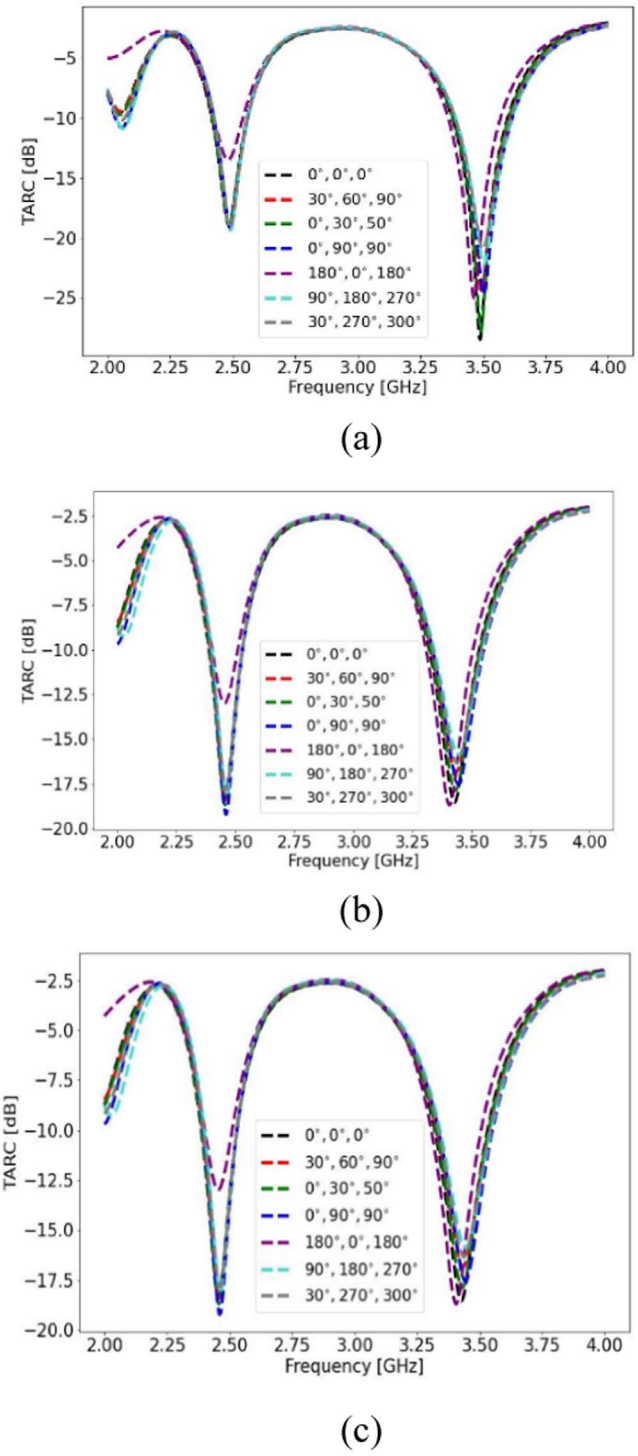

Figure 14. Total active reflection coefficient (TARC) of the MIMO antenna for bending $\theta = 60^{\circ}$ in the (a) flat, (b) x-, and (c) y-axes.

criterion (0.5) given in [21]. As seen in figure 11, a low ECC leads to a significant range gain. The DG is approximately 10 dB when the ECC value is less than 0.001. The CCL As seen in figure 12, in contrast, is the maximum expected message broadcast rate that can happen in the communication channel without causing a loss. Less than 0.4 bits/s/Hz is the permitted frequency. Figure 13 depicts the CCL calculation using (4) through (6).

It makes clear that the proposed MIMO has a suitable CCL for every functional frequency and bending scenario. We looked at the antenna parameter known as the Total Active Reflection Coefficient, or TARC for short. It is expressed as the ratio of indicated power to occurrence power in a MIMO antenna system. TARC is determined using (7) for a proposed four-port MIMO antenna and should be less than 0 dB. TARC values for the

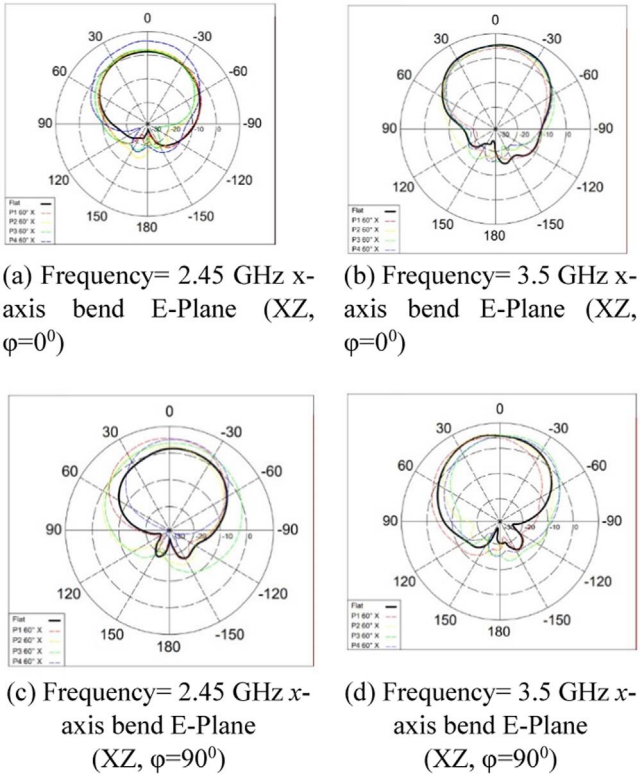

Figure 15. Radiation patterns of the proposed MIMO antenna for flat and bending $\theta = 60°$ along the x-axis. (a) Frequency = 2.45 GHz x-axis bend E-Plane (XZ, $\varphi = 0°$). (b) Frequency = 3.5 GHz x-axis bend E-Plane (XZ, $\varphi = 0°$). (c) Frequency = 2.45 GHz x-axis bend E-Plane (XZ, $\varphi = 90°$). (d) Frequency = 3.5 GHz x-axis bend E-Plane (XZ, $\varphi = 90°$).

proposed MIMO antenna were determined to be less than −5 dB at both running rates, as depicted in figure 14, are presented.

$$TARC = \frac{\sqrt{\sum_{i=1}^{N}\left| S_{i1} + \sum_{m=2}^{N} S_{im} e^{j\theta m-1}\right|^2}}{\sqrt{N}} \tag{4}$$

4.3. Radiation pattern

The recommended MIMO antenna's radiation pattern is shown in figures 15 and 16. Regardless of the frequency and port configurations (flat or bending), the primary section of the radiation pattern is provided in the forward direction with a slight inclination at $\varphi = 90°$. Furthermore, when the bending degree is = 60° at the x- and y-axes of the antenna in both the lower and higher working bands, the back lobe increases.

The antenna's achieved gain varies between 2.0 dB and 5.7 dB in the horizontal x-axis and y-axis at both frequencies of 2.45 & 3.5 GHz, as depicted in figures 17(a)–(c).

4.4. A specific absorption rate (SAR) Analysis

CST MWS was used to calculate the recommended antenna's SAR values. The location of the antenna on the upper arm in relation to a scaled-down Hugo human body model is shown in figure 18, with a 1 mm space between them. SAR spreading was averaged over 10 g of tissue at 2.4 GHz and 3.5 GHz while taking 1 W of input power into account. The antenna's highest specific absorption rates (SARs) of 10 g were recorded when the antenna was positioned on the left shoulder. The SAR values were measured at 0.0113 W kg^{-1} for a frequency of 2.45 GHz and 0.0963 W kg^{-1} for a frequency of 3.5 GHz, as depicted in figure 18. The generated SAR data was compared to a cited study. The study in [35] employed the same full ground plane and textile materials and like the suggested MIMO antenna. The SAR values were reported in [35]. The power densities at the frequencies of 3.5 & 2.45 GHz were determined to be 0.5 & 0.1 W kg^{-1}, respectively, which verifies the findings obtained by simulation. The implementation of a complete ground plane efficiently restricted the SAR values of this antenna to levels below 0.1 W kg^{-1} in both frequency ranges.

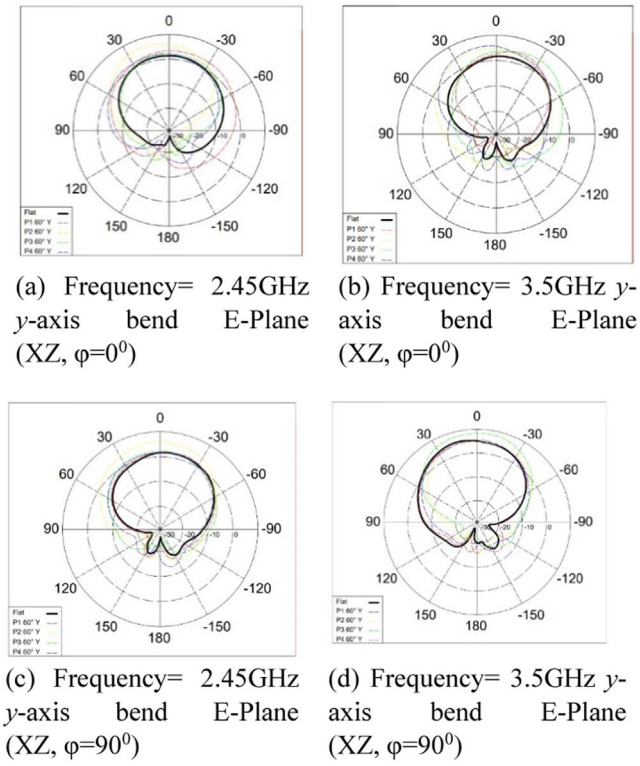

Figure 16. The Radiation patterns for the suggested MIMO antenna when bending $\theta = 60^{\circ}$ along the y-axis. (a) Frequency = 2.45 GHz y-axis bend E-Plane (XZ, $\varphi = 0^{\circ}$). (b) Frequency = 3.5 GHz y-axis bend E-Plane (XZ, $\varphi = 0^{\circ}$). (c) Frequency = 2.45 GHz y-axis bend E-Plane (XZ, $\varphi = 90^{\circ}$). (d) Frequency = 3.5 GHz y-axis bend E-Plane (XZ, $\varphi = 90^{\circ}$).

4.5. On-body evaluation

When set on the shoulder or chest as displayed in figure 18, the simulated bandwidth of the antenna in the lower band exhibits a rate of 12.4%, while the higher band demonstrates a rate of 14.2%. Simulated Sij consistently decreases to below −20 dB once the antenna is positioned on the chest or shoulder both frequency bands as shown in figure 19. Due to its low MC, The recommended antenna is appropriate for 5G and WBAN on-and off-body MIMO applications.

4.6. Fabrication and measurement results

The S-parameter of the fabricated prototype was determined by employing a Vector Network Analyzer (VNA) with the model N5227A as demonstrated in figure 20. The frequency range that this specific analyzer can operate in is 10 MHz to 67 GHz. Satimo-Starlab is utilized to evaluate the prototype's radiation pattern, a measurement system consisting of 16 reference antennas. Figures 20 and 21 depict the findings of Sii and Sij, with solid lines indicating the simulated performance of the selected port (S11) and dotted lines reflecting measured performance. The four identical antenna components exhibit a constant impedance bandwidth of 12.2% (2.36–2.65 GHz), as shown in figure 20. This almost matches the single-element flexible antenna's impedance bandwidth, demonstrating the design's viability for a MIMO configuration. The impedance bandwidth of other antennas cannot be negatively impacted by individual antenna components, demonstrating the design's applicability for real-world implementation. The proposed MIMO antenna's measured Sii shows a little variation in the flat state resonant peak. Nonetheless, when comparing the simulated and measured findings, the impedance bandwidth remains almost constant. The measured Sii for $\theta = 60^{\circ}$ bending configurations along the x- and y-axes agree with the flat condition. When curved at the most severe situation ($\theta = 60^{\circ}$ at the y-axis), the suggested MIMO antenna provided a minor downward shift in the lower and higher bands (S33 and S44). The simulated (S21) and measured (S12, S13, S14, S23, S24, S34) MC are illustrated in figures 21(a)–(c), respectively. The testing antenna is placed at the central point inside this setup. With a bending angle of $\theta = 60^{\circ}$, figure 22 shows the measurement of the suggested MIMO antenna both flat and bent. The MC level of all port configurations is well below 20 dB under flat conditions for simulated and measured results. Once the antenna is curved along the x- and y-axes ($\theta = 60^{\circ}$) within the lower and upper frequency ranges, the measured values of S13, S14, S23, S24, and S34 are consistently less than −20 dB. This implies that the MC is greatly lowered, even

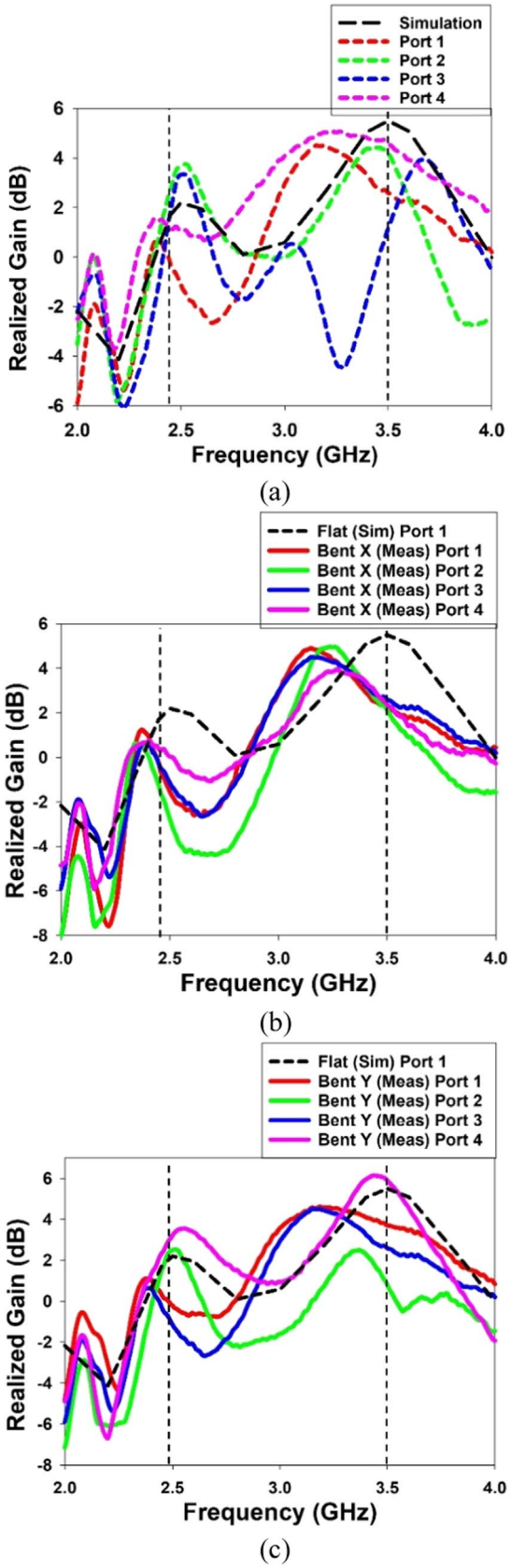

Figure 17. The gain was measured under various bending circumstances along the *y*-axis and *x*-axis. (a) 2.45 GHz (b) 3.5 GHz.

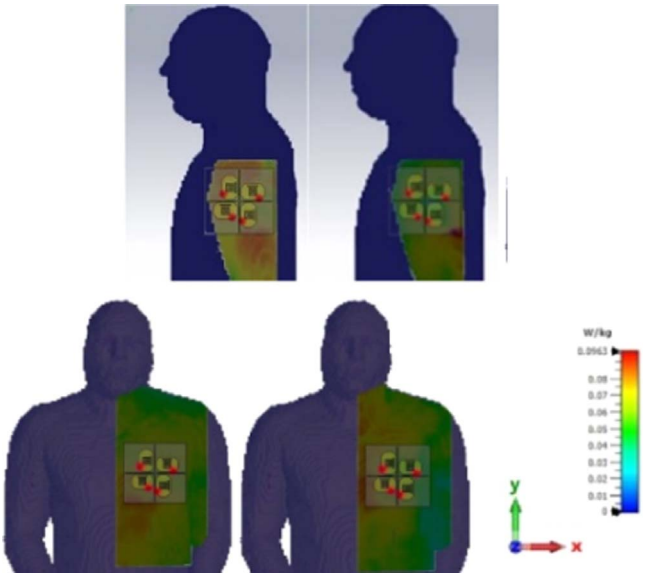

Figure 18. SAR assessment of the left upper arm at 10 g on the Hugo body model. SAR assessment at 2.45 GHz (a) and 3.5 GHz (b) on the Hugo body model at 10 g on the chest. 3.5 GHz and 2.45 GHz (c) (d).

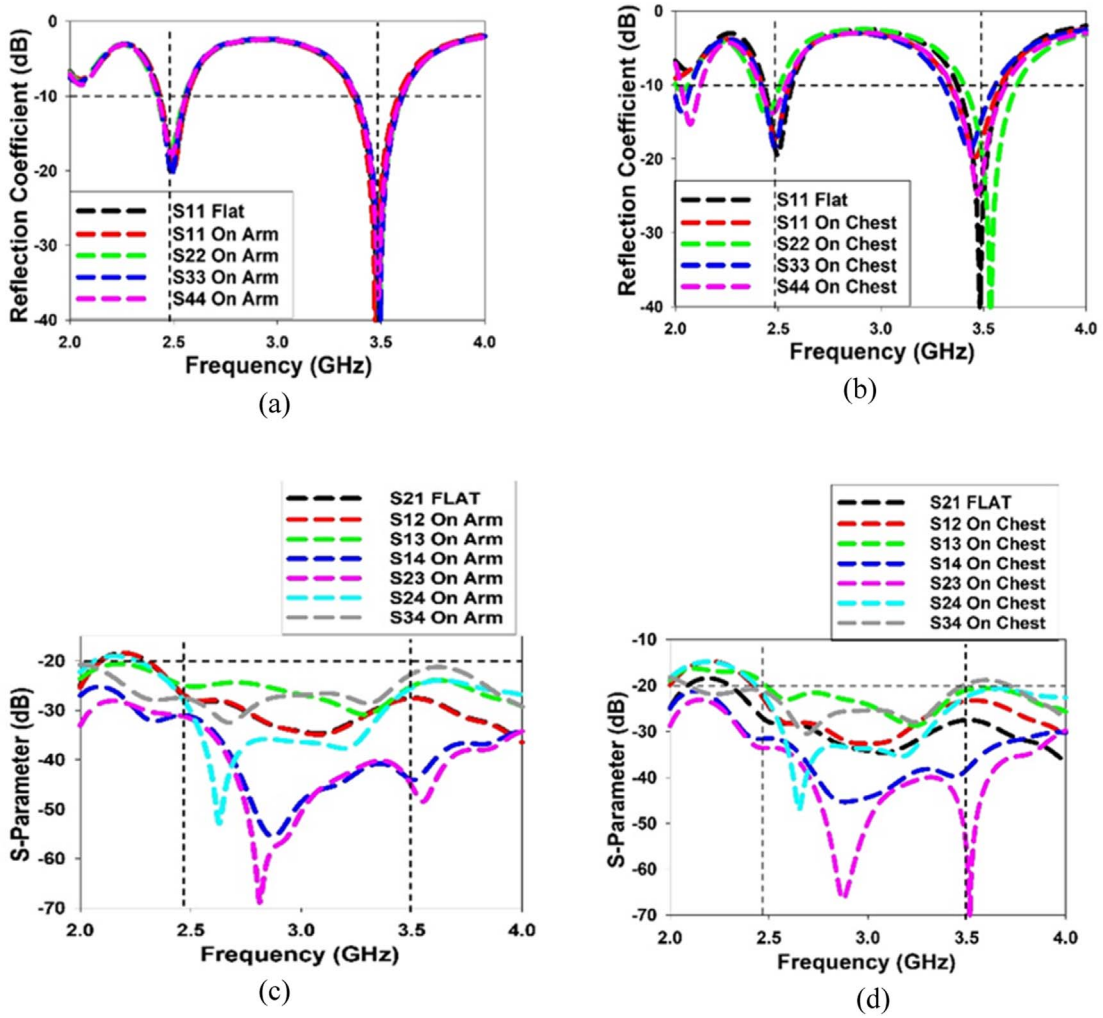

Figure 19. On-body simulation results of the suggested MIMO. (a) Sii antenna on shoulder, (b) Sii antenna on chest, (c) Sij antenna on the shoulder and (d) Sij antenna on chest.

Table 4. Compares the MIMO antenna to a few antennas state-of-the-art structures.

References	Sub. Material	Antenna Categories	Dimensions (mm × mm)	Operating Freq. (GHZ)	Gain (dB)	MC (dB)	Edge to edge (mm)	ECC
[8]	FR4	Isolation	40 × 40	3.4—3.6	2.4	−35	NA	< 0.001
[14]	Paper	Bandwidth	40 × 110	2.22–3.85	2	NA	5	$< 0.2 \times 10^{-6}$
[20]	Jeans denim	Isolation	29 × 55	2.9–4.1	9.65	−19	14	< 0.2
[21]	Felt ($\varepsilon_r = 1.2$)	Isolation	140 × 70	2.33–2.51	4.7	−25	10.4	< 0.001
[36]	Felt ($\varepsilon_r = 1.44$)	Isolation	140 × 70	2.45	4.7	< −26	10.4	< 0.5
[37]	Felt ($\varepsilon_r = 1.3$)	Bandwidth	44.1 × 44.1	2.45 & 5.5	0.67 & 7.4	25	NA	NA
[38]	FR4	Isolation	42 × 42	3.09 ∼ 12	2 ∼ 5.1	< −16.4	NA	< 0.01
[39]	Jeans	Isolation	40 × 50	4.35–7	6.74	< −28.5	25	< 0.025
This work	Felt	Isolation	132.8 × 127.6	2.45,3.5	1.87 & 5.48	(< −20)	5.2	< 0.002

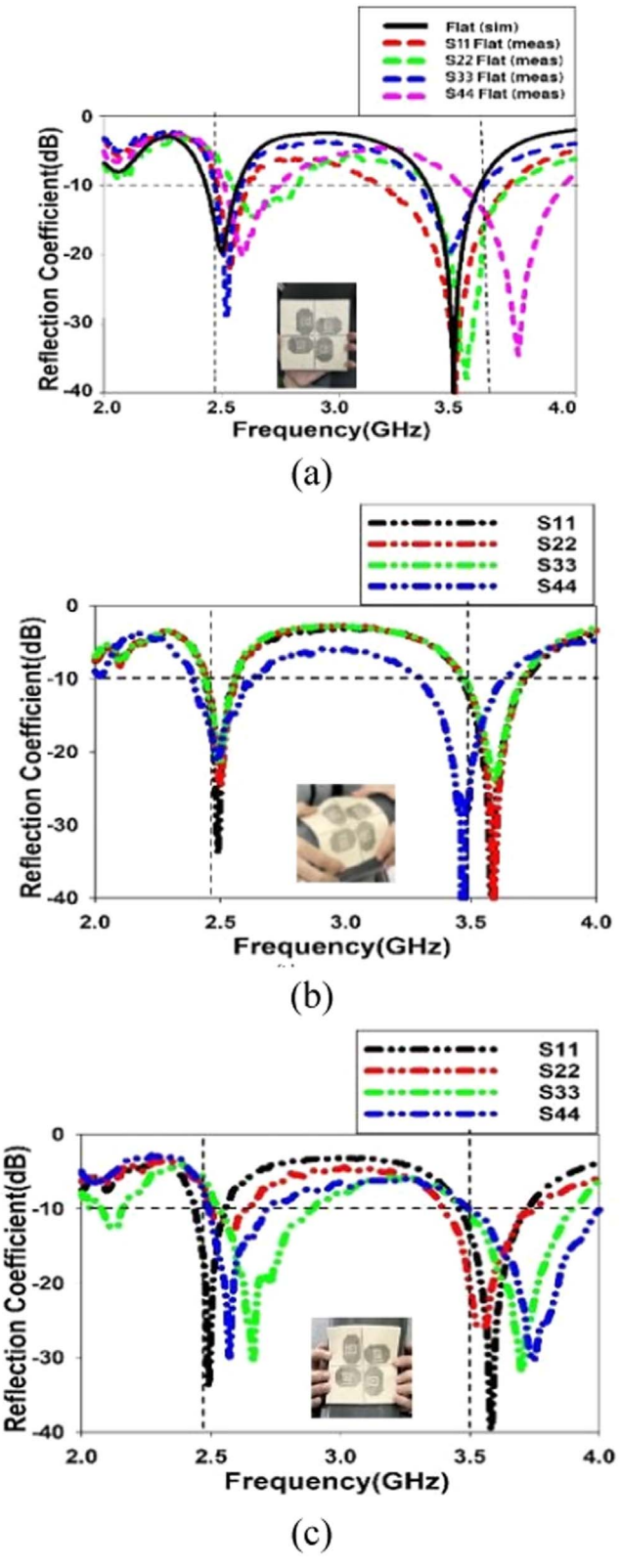

Figure 20. Reflection coefficient of the four-port flexible MIMO antenna: (a) simulated and measured sii flat, (b) measured sii *x*-axis bend (c) measured sii *y*-axis bend.

under the critical bending situation. The suggested antenna offers the novelty of dual-band frequency at 3.5 GHz and 2.45 with four-port, smaller gaps between edge-to-edge antenna patch elements, higher gain and low ECC compared with reported studies as listed in table 4.

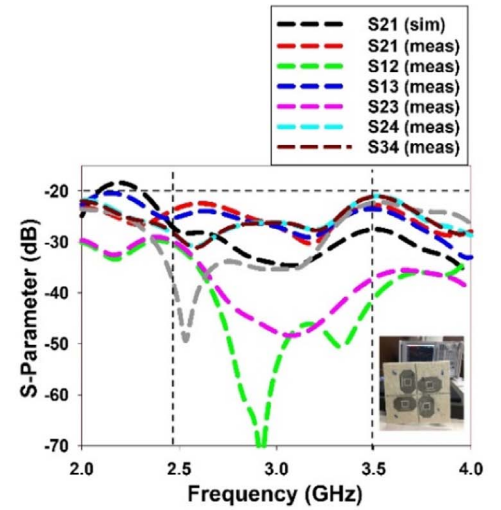

(a)

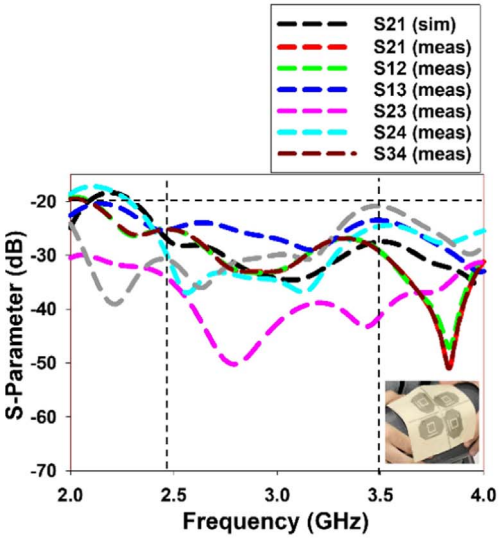

(b)

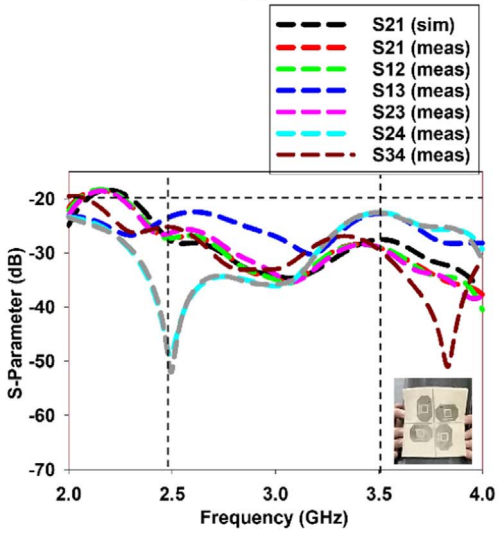

(c)

Figure 21. A comparison of the proposed MIMO antenna's measured and simulated S-parameters: Sij *x*-axis bend (b) and Sij flat (a) (c) Bend in Sij *y*-axis.

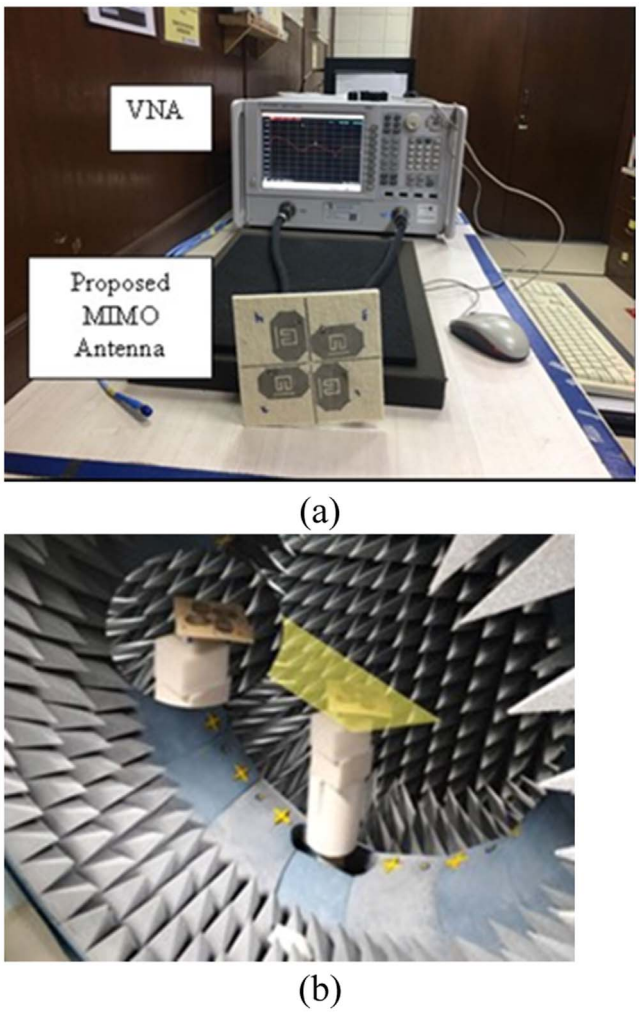

Figure 22. Measurement setup (a) Antenna measurement using Vector Network Analyzer (b) Field antenna measurement setup in an Anechoic Chamber.

5. Conclusion

This paper presents the proposed unique structure of a flexible square and bar-slotted 4-port MIMO textile antenna based on hybrid MC technique to reduce MC for on-body use. The modelling and findings agree well, and the revised structure is simple to construct as a textile antenna. When the antenna's performance is evaluated under various bending directions and bend intensities, it is revealed that the antenna's radiation, MC, and reflection coefficient characteristics vary only a little. Additionally, the MIMO constraints evaluation of features like TARC, DG, CCL, and ECC supports the idea that this antenna may be used in the upcoming 5G wearable technology. Upcoming work will be foreseen by implanting, collecting, and analyzing data from a certain phantom with a tumor.

5.1. Future work

Multiband MIMO textile antenna for mmWave 5G applications While the study focused on the antenna's performance at 2.45 GHz and 3.5 GHz, it would be helpful to investigate its performance over a wider variety of mmWave frequency bands. This will provide a comprehensive understanding of the antenna's capabilities and limitations in various frequency ranges.

Compactness and optimization of antenna design Explore further optimization techniques to enhance the performance of the proposed antenna. This could involve fine-tuning the dimensions, shapes, and materials used in the antenna structure to achieve even better results.

Acknowledgments

This study is supported via funding from Prince sattam bin Abdulaziz University project number (PSAU/2024/R/1445).

Data availability statement

The data cannot be made publicly available upon publication because no suitable repository exists for hosting data in this field of study. The data that support the findings of this study are available upon reasonable request from the authors.

ORCID iDs

Hamza A Mashagba https://orcid.org/0000-0002-2952-2617
Hasliza A Rahim https://orcid.org/0000-0002-5662-7158
Mohammad Tariqul Islam https://orcid.org/0000-0002-4929-3209
Wazie M Abdulkawi https://orcid.org/0000-0002-7593-5359
Samir Salem Al-Bawri https://orcid.org/0000-0003-2852-575X

References

[1] Rahim H A, Abdulmalek M, Soh P J and Vandenbosch G A E 2017 Evaluation of a broadband textile monopole antenna performance for subject-specific on-body applications *Appl. Phys.* A **123** 1–6
[2] Asif M, Sehrai D A, Kiani S H, Khan J, Abdullah M, Ibrar M and Limiti E 2021 Design of a dual band SNG metamaterial based antenna for LTE 46/WLAN and Ka-band applications *IEEE Access* **9** 71553–62
[3] Nouri M, Abazari Aghdam S, Jafarieh A, Mallat N K, Jamaluddin M H and Dor-Emami M 2021 An optimized small compact rectangular antenna with meta-material based on fast multi-objective optimization for 5G mobile communication *J. Comput. Electron.* **20** 1532–40
[4] Singh A K and Raman A 2018 Multiband microstrip patch antenna design for 5G using metamaterial structure *2018 2nd Int. Conf. on Trends in Electronics and Informatics (ICOEI)* (IEEE) pp 909–14
[5] Vinoth M and Vallikannu R 2021 Design and analysis of metamaterial patch antenna 5G and X band applications *2021 Int. Conf. on Computer Communication and Informatics (ICCCI)* (IEEE) pp 1–6
[6] Mashagba H A, Rahim H A, Adam I, Jamaluddin M H, Yasin M N M, Jusoh M and Soh P J 2021 A hybrid mutual coupling reduction technique in a dual-band MIMO textile antenna for WBAN and 5G applications *IEEE Access* **9** 150768–80
[7] Chouikhi L, Essid C, Sakli H and Salah B B 2021 Metamaterial decoupling MIMO antennas for 5G communication *2021 Int. Conf. on Software, Telecommunications and Computer Networks (SoftCOM)* (IEEE) pp 1–6
[8] Anbarasu M and Nithiyanantham J 2023 Performance analysis of highly efficient two-port MIMO antenna for 5G wearable applications *IETE Journal of Research* **69** 3594–603
[9] Alhawari A R, Saeidi T, Almawgani A H M, Hindi A T, Alghamdi H, Alsuwian T and Imran M A 2021 Wearable metamaterial dual-polarized high isolation UWB MIMO vivaldi antenna for 5G and satellite communications *Micromachines* **12** 1559
[10] Khan J, Ullah S, Ali U, Tahir F A, Peter I and Matekovits L 2022 Design of a millimeter-wave MIMO antenna array for 5G communication terminals *Sensors* **22** 2768
[11] Raj T, Mishra R, Kumar P and Kapoor A 2023 Advances in MIMO antenna design for 5G: a comprehensive review *Sensors* **23** 6329
[12] Adam I, Yasin M N M, Ramli N, Jusoh M, Rahim H A, Latef T B A and Sabapathy T 2019 Mutual coupling reduction of a wideband circularly polarized microstrip MIMO antenna *IEEE Access* **7** 97838–45
[13] Salarrahimi M, Volski V and Vandenbosch G A 2019 Mutual coupling-based compact wideband circularly polarized antenna *IEEE Trans. Antennas Propag.* **67** 4872–7
[14] Kumar P, Urooj S and Malibari A 2020 Design of quad-port ultra-wideband multiple-input-multiple-output antenna with wide axial-ratio bandwidth *Sensors* **20** 1174
[15] Khurshid A, Dong J, Ahmad M S and Shi R 2022 Optimized super-wideband MIMO antenna with high isolation for IoT applications *Micromachines* **13** 514
[16] Jiang X, Wang H and Jiang T 2017 A low mutual coupling MIMO antenna using EBG structures *2017 Progress In Electromagnetics Research Symp.-Spring (PIERS)* (IEEE) pp 660–3
[17] Dabas T, Gangwar D, Kanaujia B K and Gautam A K 2018 Mutual coupling reduction between elements of UWB MIMO antenna using small size uniplanar EBG exhibiting multiple stop bands *AEU-Int. J. Electron. Commun.* **93** 32–8
[18] Zhang S and Pedersen G F 2015 Mutual coupling reduction for UWB MIMO antennas with a wideband neutralization line *IEEE Antennas Wirel. Propag. Lett.* **15** 166–9
[19] Marzudi W N N W, Abidin Z Z, Muji S Z M, Yue M and Abd-Alhameed R 2014 Minimization of Mutual Coupling Using Neutralization Line Technique for 2.4 GHz Wireless Applications *International Journal of Digital Information and Wireless Communications (IJDIWC)* **4** 292–8
[20] Roy S and Chakraborty U 2020 Mutual coupling reduction in a multi-band MIMO antenna using meta-inspired decoupling network *Wirel. Pers. Commun.* **114** 3231–46
[21] Adam I, Rahim H A, Yasin M N M and Nasrol M N M 2021 Mutual coupling suppression in wearable MIMO antenna for on/off-body WBAN applications *Journal of Physics: Conf. Series* 1755 (IOP Publishing) 012011
[22] Kumar Biswas A and Chakraborty U 2019 Compact wearable MIMO antenna with improved port isolation for ultra-wideband applications *IET Microw. Antennas Propag.* **13** 498–504

[23] Luo C M, Hong J S and Amin M 2017 Mutual coupling reduction for dual-band MIMO antenna with simple structure *Radioengineering* **26** 51–6
[24] Zhang J, Yan S, Hu X and Vandenbosch G A 2019 Reduction of mutual coupling for wearable antennas *2019 13th European Conf. on Antennas and Propagation (EuCAP)* (IEEE) pp 1–2
[25] Zhang J, Yan S, Hu X and Vandenbosch G A 2019 Mutual coupling suppression for on-body multiantenna systems *IEEE Trans. Electromagn. Compat.* **62** 1045–54
[26] Iqbal J, Illahi U, Sulaiman M I, Alam M M, Su'ud M M and Yasin M N M 2019 Mutual coupling reduction using hybrid technique in wideband circularly polarized MIMO antenna for WiMAX applications *IEEE Access* **7** 40951–8
[27] Elfergani I, Iqbal A, Zebiri C, Basir A, Rodriguez J, Sajedin M and Ullah S 2020 . Low-profile and closely spaced four-element MIMO antenna for wireless body area networks *Electronics* **9** 258
[28] Iqbal A, Smida A, Alazemi A J, Waly M I, Mallat N K and Kim S 2020 Wideband circularly polarized MIMO antenna for high data wearable biotelemetric devices *IEEE Access* **8** 17935–44
[29] Alibakhshikenari M, Babaeian F, Virdee B S, Aïssa S, Azpilicueta L, See C H and Limiti E 2020 A comprehensive survey on 'Various decoupling mechanisms with focus on metamaterial and metasurface principles applicable to SAR and MIMO antenna systems *Ieee Access* **8** 192965–3004
[30] Nadeem I and Choi D Y 2018 Study on mutual coupling reduction technique for MIMO antennas *IEEE Access* **7** 563–86
[31] Liao C T, Yang Z K and Chen H M 2021 Multiple integrated antennas for wearable fifth-generation communication and internet of things applications *IEEE Access* **9** 120328–46
[32] Rahim H A, Malek F, Soh P J, Romli A, Abd Rani K, Isa C M N C and Fuad F A A 2017 Measurement of dielectric properties of textile substrate *Journal of Engineering and Applied Sciences* **12** 4311–2
[33] Mohammad E A, Rahim H A, Soh P J, Jamlos M F, Abdulmalek M and Lee Y S 2018 Dual-band circularly polarized textile antenna with split ring slot for off-body 4G LTE and WLAN applications *Appl. Phys.*A **124** 1–10
[34] Roy S, Biswas A K, Ghosh S, Chakraborty U and Sarkhel A 2021 Isolation improvement of dual-/quad-element textile MIMO antenna for 5G application *J. Electromagn. Waves Appl.* **35** 1337–53
[35] Soh P J, Vandenbosch G, Wee F H, van den Bosch A, Martinez-Vazquez M and Schreurs D 2015 Specific absorption rate (SAR) evaluation of textile antennas *IEEE Antennas Propag. Mag.* **57** 229–40
[36] Adam I, Kamarudin M R, Rambe A H, Haris N, Rahim H A, Wan Muhamad W Z A and Yasin M N M 2021 Investigation on wearable antenna under different bending conditions for wireless body area network (WBAN) applications *International Journal of Antennas and Propagation* **2021** 5563528
[37] Zhang K, Soh P J and Yan S 2022 Design of a compact dual-band textile antenna based on metasurface *IEEE Trans. Biomed. Circuits Syst.* **16** 211–21
[38] Wu A, Tao Y, Zhang P, Zhang Z and Fang Z 2023 A compact high-isolation four-element MIMO antenna with asymptote-shaped structure *Sensors* **23** 2484
[39] Pradeep P, Basha M M, Gundala S and Syed J 2024 Development of wearable textile MIMO antenna for Sub-6 GHz band new radio 5G applications *Micromachines* **15** 651